An in vitro comparison of the hemodynamics of two inferior vena cava filters

Gregory G. Couch, MASc, K. Wayne Johnston, MD, FRCS, and Matadial Ojha, PhD, *Toronto, Canada*

Purpose: The effectiveness of an inferior vena cava (IVC) filter in preventing pulmonary embolism while preserving caval flow is significantly affected by its hemodynamic characteristics. Flow fields surrounding two types of IVC filters were compared to assess how the design of a filter may influence performance.
Methods: The 12F Titanium Greenfield and VenaTech LGM inferior vena cava filters were studied in vitro with a noninvasive flow visualization technique, the photochromic flow visualization and measurement technique. Axial velocity profiles and wall shear stress distributions were measured. These results were compared with analytical data corresponding to the flow field in the absence of a filter to determine the relative extent of the flow disturbances.
Results: The reductions in near-wall axial velocity and wall shear stress caused by the VenaTech filter were more extensive and severe than those caused by the Greenfield filter. These changes were the consequence of differences in the geometry and dimensions of the struts of the two filters. The measurements showed the flow fields to be laminar, with no evidence of turbulence in both cases.
Conclusion: Two factors that have been linked to thrombogenesis, near-wall velocity and wall-shear stress, were significantly affected by the larger frontal profile area of the VenaTech filter. Although a larger area may increase clot-trapping efficiency, as shown by previous studies, the reduced near-wall velocities and wall shear stresses may increase the potential for thrombogenesis and, thus, caval occlusion. In contrast to other in vitro flow visualization studies, no turbulence was observed with either filter. (J Vasc Surg 2000;31:539-49.)

The effectiveness of an inferior vena cava (IVC) filter in preventing pulmonary embolism has been widely demonstrated.[1-8] Because of the advantages offered by percutaneous insertion over transvenous placement, a number of different designs are being marketed for clinical use.

Because the IVC filter is designed to prevent the migration of emboli to the pulmonary circulation and also maintain IVC patency by promoting lysis of clots within the filter, it is likely that the flow field induced by the filter significantly influences the actions of entrapment and lysis. A number of comparative trials have been conducted with various filter designs to determine their relative effectiveness.[3,9,10] In most of the studies that have examined the flow dynamics in the region of the filter, the results have been mostly qualitative, because of the limitations of the flow visualization and measurement techniques that were used.[11-14] Dye injection was commonly used as a means of visualizing the flow effect of various filters.

From the Institute of Biomedical Engineering, Department of Chemical Engineering and Applied Chemistry (Mr Couch and Dr Ojha), and Department of Surgery (Drs Johnston and Ojha), University of Toronto.
Supported by a contract from Boston Scientific Corporation (to Dr Ojha).
Competition of interest: M.O. is supported by a contract from Boston Scientific Corporation.
Reprint requests: Professor Matadial Ojha, Institute for Biomedical Engineering, University of Toronto, 4 Taddle Creek Rd, Toronto, Ontario, Canada M5S 369.

0741-5214/2000/$12.00 + 0 24/1/103799
doi:10.1067/mva.2000.103799

Because this technique is invasive, dye must be injected at an appropriate upstream location to avoid affecting the flow field at the desired site of observation. Consequently, the streamline or traces formed by the dye is an integration of the effects of the flow field along its path. This factor, combined with the complexity of the flow fields, limited the comparisons among the different filter designs to a qualitative description of the degree of "turbulence," based on subjective estimates of the extent of mixing of the injected dye stream.

In this study, the flow fields generated by two different vena cava filter designs, the 12F Titanium Greenfield and the VenaTech LGM, were measured with the photochromic flow visualization and measurement technique. Each filter was examined in an unoccluded state (ie, with no entrapped emboli) in an idealized model of an IVC. The results were compared to determine the relative hemodynamic effects of the filters. We used this technique in an earlier study to determine the influence of a trapped embolus on the velocity and shear stress fields.[15]

METHODS

Because the flow field surrounding an IVC filter is complex and three-dimensional, a detailed hemodynamic assessment presents a considerable technical challenge. Conventional flow measurement techniques are limited in their ability to accurately characterize complex flow fields, especially near solid boundaries. Even with advanced techniques such as laser Doppler anemometry, difficulties with optical interference may be encountered, because significant portions of the hemodynamic interaction with a filter take place in the vicinity of solid boundaries (ie, the vessel wall and the filter "legs" and apex). The photochromic dye tracer technique was chosen to overcome these difficulties.

The photochromic flow visualization and measurement technique. The photochromic flow visualization and measurement technique uses a colorless indicator that becomes opaque when exposed to ultraviolet light. This reversible photochemical reaction is used to instantaneously "tag" the fluid molecules. When the motion of these "tagged" elements are tracked, the flow field can be characterized, and various fluid dynamic quantities, including velocity and wall shear stress, can be deduced. Extensive use has been made of the photochromic technique in a variety of in vitro studies.[15-18]

The photochromic flow visualization and measurement system used in this study consisted of these major components: a pulsed nitrogen laser (λ = 337 nm), a convex lens (f = 380 mm), an electronic strobe, a high resolution charge-coupled device (CCD) camera with a digital interface (Kodak MegaPlus 1.4), a macro lens and bellows system, a digital frame grabber (DIPIX P360, Ottawa, Ontario), a motorized stage and controller, a programmable waveform pump (UHDC, London, Ontario), and a computer (IBM 486 PC compatible) for the control and synchronization of the individual components of the system and to record and analyze images from the CCD camera (Fig 1).

The in vitro flow model or phantom and the filter were mounted on the motorized stage and positioned for the path of the laser beam. This beam was focused by means of the convex lens to produce a dye trace within the flow field surrounding the filter. Because the filter and flow phantom were mounted on the motorized stage, traces could be recorded at any desired position within the flow field.

Flow model construction. The photochromic tracer method requires the use of a UV transparent flow phantom or test section. Because UV transparent Plexiglas of sufficient thickness was not commercially available, we constructed the test section (Fig 2) by polymerizing methylmethacrylate monomer. The mold was made in the form of a straight tube with an internal diameter of 20 mm and a notch to allow for the proper positioning and centering of the Greenfield filter. A flexible insert for the notch was made of Sylgard to allow for the embedding of the filter hooks or "feet" into the vessel wall. With the filter "feet" properly positioned (Fig 2, *A*), the flow field near the vessel wall should more accurately reflect the in vivo situation.

However, in the case of the VenaTech LGM filter (Fig 2, *B*), the "feet" extend its entire length and would obscure the CCD camera's view of the flow field and the path of the laser beam. Therefore, sections of the "feet" were removed where necessary. The removal of these sections should not significantly alter the surrounding flow field, because the feet of the filter lie flush with the vessel wall, where they would have had little or no effect.

The entrance length of the flow phantom was 80 tube diameters (160 cm), to ensure that the flow was fully developed upstream of the filter base and that the velocity profile was parabolic under steady flow (Poiseuille flow). These inlet conditions were confirmed with the photochromic method; errors in the measured centerline velocities upstream of the filter were less than 1%.

Because the flow field generated by the filters was expected to be three-dimensional and asymmet-

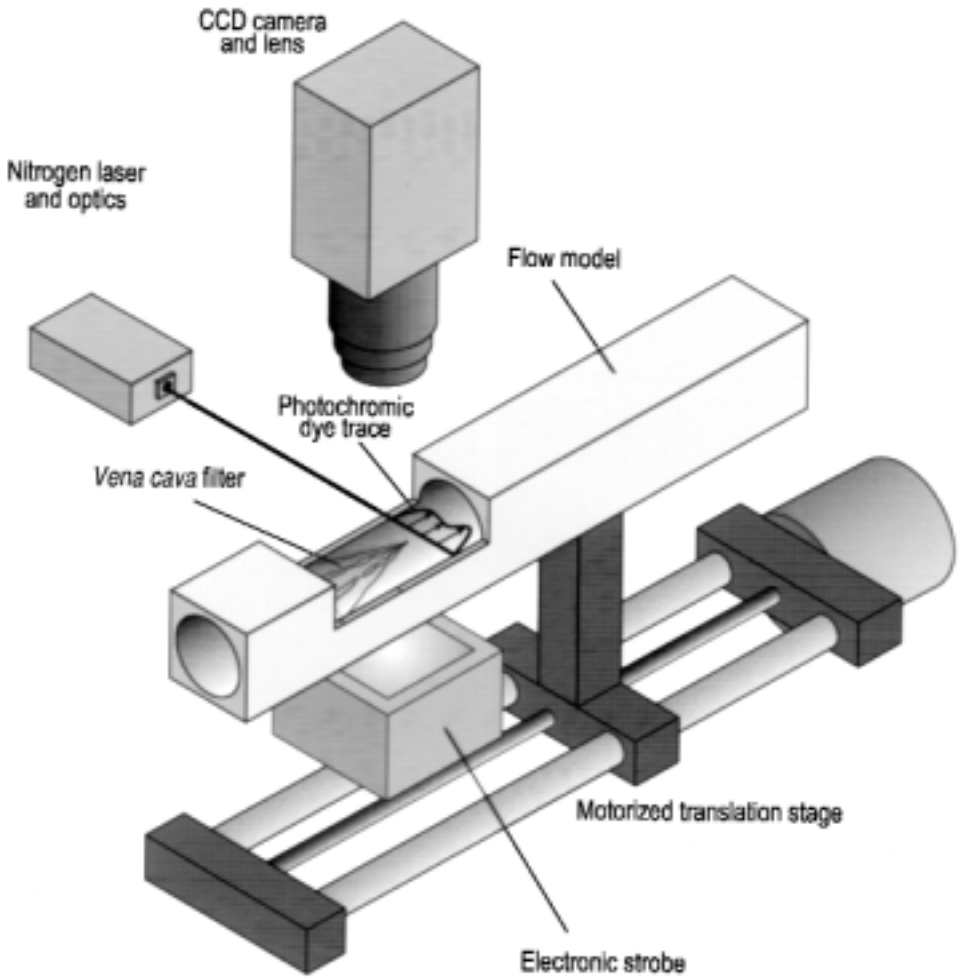

Fig 1. The photochromic flow visualization and measurement system. *CCD,* Charge-coupled device.

ric, we conducted measurements in several planes passing through the longitudinal axis. The test section was mounted in a carrier designed to rotate around its longitudinal axis, allowing any desired plane to be examined to facilitate this experimental requirement.

Flow conditions. The test fluid used in these experiments was a solution of Shell-Sol 715 and 50 ppm of photochromic dye (l′,3′,3′-trimethylindoline-6-nitro-benzospiropyran). With a kinematic viscosity of 1.8 centiStoke (cS) and density of 0.76 g/mL, this fluid has different physical properties than that of blood (υ = 3.5 cS, ρ = 1.01 g/mL) or the fluids used in previous work.[11-14] However, based on the principle of dynamic similarity, the in vivo flow field was simulated by adjusting the flow rate to match the Reynolds number. In these experiments, the Reynolds number was defined for the flow rate, Q, and the diameter of the vessel, D, and the kinematic viscosity, ν, and is given by:

$$\mathrm{Re} = \frac{4Q}{\pi \nu D}$$

Thus, an in vitro flow rate of approximately 1 L/min was used to compensate for the different physical properties of the test fluid. This flow rate corresponds to a Reynolds number of 600, the approximate time-averaged in vivo value.

RESULTS

Measurements were made in horizontal and perpendicular planes passing through the longitudinal axis of the test section to observe the effects of any asymmetry in the flow field generated by a filter. The spatial resolution of the measurements was increased by adjusting the magnification of the CCD camera so

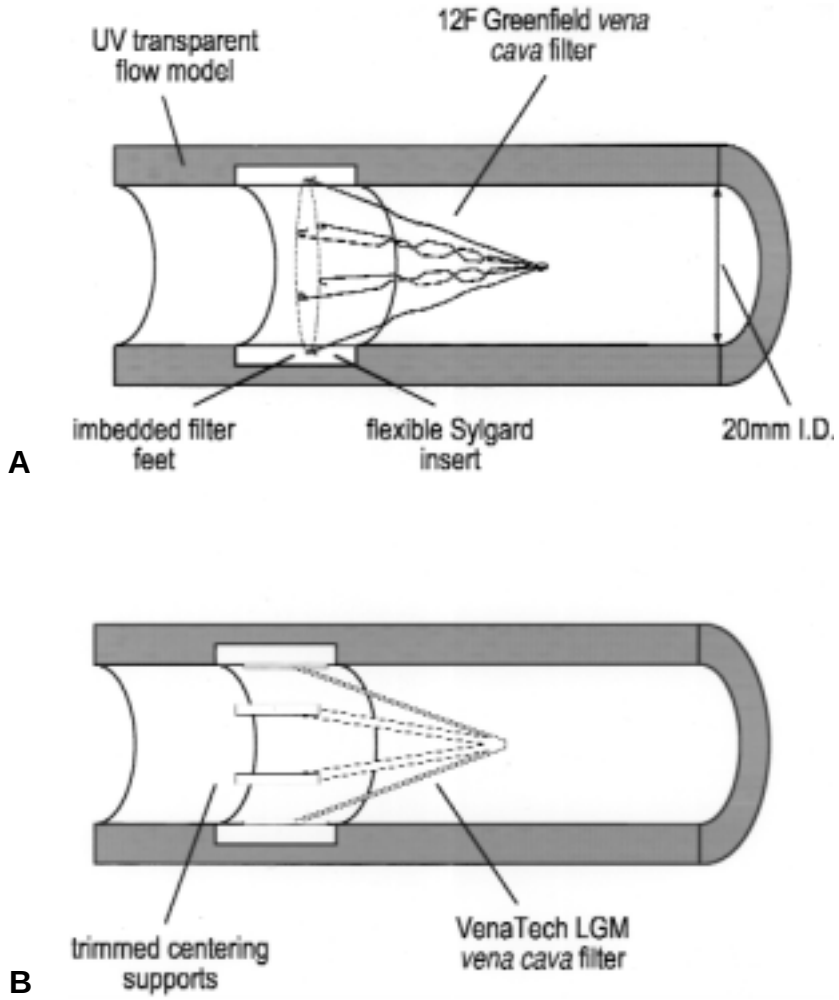

Fig 2. Flow phantom and insertion of A, the 12F Titanium Greenfield filter, and B, the VenaTech LGM filter

that its field of view encompassed slightly more than half of the inner diameter of the tube, or 10 mm, extending from the center to the inner wall (Fig 3).

A total of four separate scans along the longitudinal axis were made for each filter, starting from the base to a position lying several tube diameters downstream of the tip. In between scans, the flow phantom was rotated around its longitudinal axis by 90 degrees. Consequently, the first and third scans lie in one plane, whereas the second and fourth scans lie in a second, perpendicular plane. The orientation and numbering scheme used to identify these scans is shown in Fig 4.

Each scan was composed of several photochromic profiles recorded at 1 mm intervals along the tube axis. At each position, a photochromic trace was first formed with a flash delay of 0 ms to obtain the initial position and angle of the trace and its intersection with the wall. Then a second trace was formed with a flash delay of 20 ms. The information from the first displacement profile made it unnecessary to precisely align the beam of the laser perpendicular to the wall and allowed the velocity profile to be determined more accurately from the relative displacement between the two profiles. In addition, the positions of the intersections with the wall obtained from the first trace facilitated calculation of wall shear stress.

Displacement and velocity profiles. The displacement profiles obtained from the four scans of the Greenfield and VenaTech filters are shown in Fig 5. The profiles recorded with a flash delay of 0 ms show the initial position of the traces, whereas the second set of profiles, recorded with a delay of 20 ms, show the displacement of the traces by the flow field. Each displacement profile represents the mean of 10 traces.

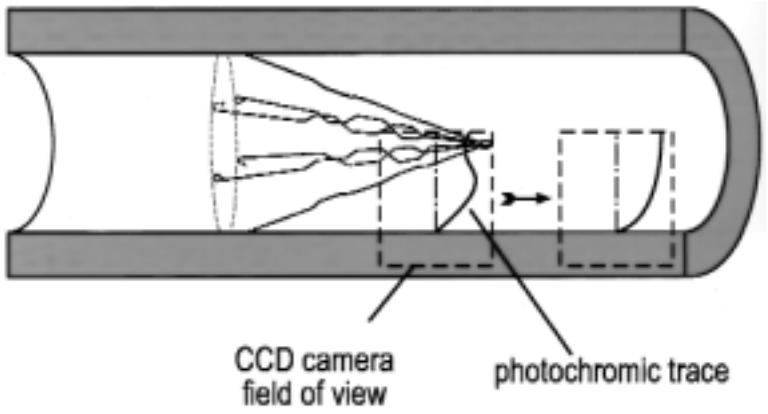

Fig 3. Direction of the scan with the photochromic system, and the field of view of the charge-coupled device camera.

Within the interior of the filters, some noise is evident in the measured profiles, because the algorithm used by the automated imaging system did not detect the photochromic trace. Failure was primarily caused by the filter "legs" preventing the penetration of the trace. In other instances, poor trace contrast or image artifacts prevented a trace profile from being detected properly. The noise does not represent chaotic or turbulent flow, because such noise was present for traces recorded with a flash delay of 0 ms, corresponding to zero displacement by the flow, and also because the disturbed region was confined to a small portion of the interior of the filter. Any disturbed or turbulent flow produced within the filter cone would also be seen downstream of the filter, because such flow features are usually dissipated over several vessel diameters.

In Fig 5*C*, the axial velocity profiles calculated from the relative displacements of the two sets of displacement profiles are shown for the two filters. The parabolic velocity profile representing the flow in the absence of the filter is superimposed over each experimentally measured profile to demonstrate a filter's effect on the surrounding flow field. This theoretical profile is given by:

$$u(r) = \frac{32Q}{\pi} \frac{R^2 - r^2}{D^4}$$

in which u is the axial velocity, r is the radial distance to the center of the tube, Q is the flow rate, and D is the diameter of the vessel. This profile is based on the analytical solution to the Navier Stokes equation for flow in a straight tube, ie, Poiseuille flow, and is calculated assuming the same flow rate that is used with the filter. For comparison, the maximum velocity (10.8 cm / sec) of the theoretical profile occurs at the centerline. In vivo, this would correspond to a velocity of approximately 20.5 cm / sec.

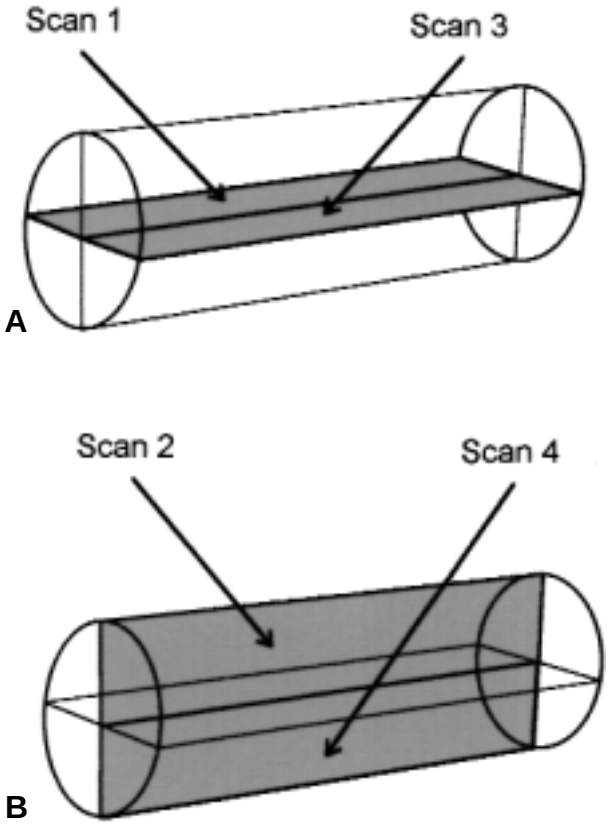

Fig 4. Spatial orientation and numbering convention used to identify the four scans within the flow phantom.

Excellent agreement between the experimental and predicted velocities was revealed by means of a comparison of these profiles upstream of the base of the filters. Corresponding experimental and theoret-

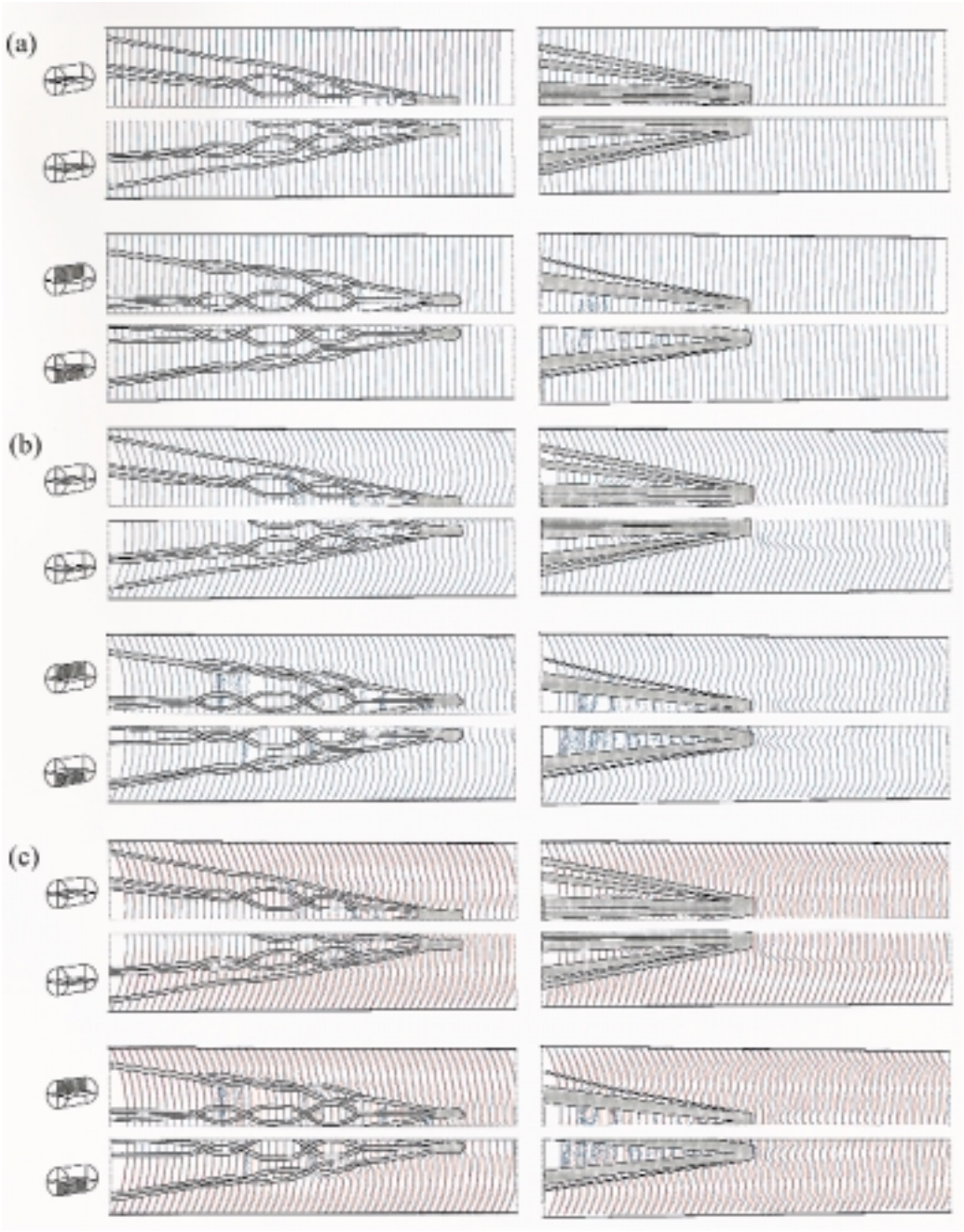

Fig 5. Displacement profiles (*blue*) recorded in the 12F Greenfield (*left*) and VenaTech LGM filters (*right*) A, with a flash delay of 0 ms, B, with a flash delay of 20 ms, and C, superimposed with theoretical velocity profiles (*red*) for flow in the absence of the filter for comparison. Each profile represents the average of 10 measurements.

ical profiles always coincide at the intersection with the wall, because of the assumption of the no-slip condition (ie, the fluid velocity is zero at the wall) to assist in the comparison.

As explained earlier, our flow conditions were matched to the in vivo conditions, based on the Reynolds number of 600. The measured or in vitro velocities are related to in vivo values by this expression:

$$\left(\frac{u}{v}\right)_{\text{in vivo}} = \left(\frac{u}{y}\right)_{\text{in vivo}}$$

in which u is the axial velocity and v is the kinematic viscosity. Thus, based on the physical properties of

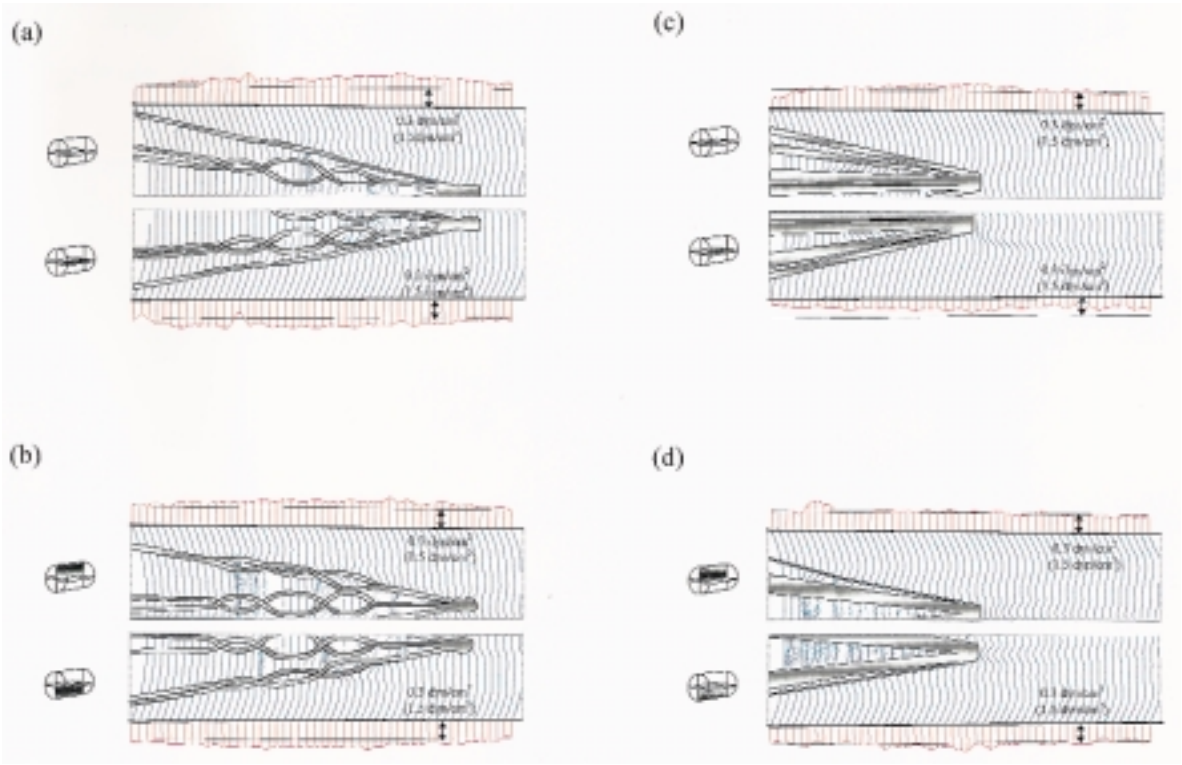

Fig 6. Wall shear stress distributions measured in A, the horizontal and B, the vertical cross-sectional planes of the 12F Titanium Greenfield filter, and in C, the horizontal and D, the vertical cross-sectional planes of the VenaTech LGM filter. For comparison, the theoretical wall shear stress in the absence of the filter is shown.

blood and the test fluid given earlier, the in vitro velocities must be multiplied by a factor of 1.9 to obtain the corresponding in vivo values.

If the two sets of profiles from each plane are examined carefully, it is clear that the profiles do not coincide or overlap at the center of the flow and that one set of profiles is shifted slightly downstream. This resulted from misalignment of the laser beam when the vessel was rotated by 180 degrees for the second scan in the same plane. As expected, this misalignment is most apparent at the center of the flow field. Nevertheless, it has no effect on the accuracy of the velocity or wall shear stress measurements for the indicated trace positions.

No significant deviations in velocity profiles upstream of the base of the filter were revealed by means of the results for the Greenfield filter. Downstream of the base, the filter struts or "legs" were seen to affect the velocity field by obstructing the flow at various positions. These disturbances occurred where the "legs" intersected the plane of measurement and extended for more than one tube diameter downstream, as evidenced by the reduced velocities apparent in the shadow of the "leg." These interactions were seen in all scans, but at differing positions because of the asymmetry of the filter. Continuing downstream, the effect of the tip of the filter is observed, followed by the gradual redevelopment of the parabolic flow field.

The results for the VenaTech filter show a similar interaction of the filter "legs" with the flow field. All the scans show substantially reduced velocities downstream of the base of the filter. The most significant deviation from a parabolic velocity profile is observed in scan 3 (Fig 5,*C*), in which a region of substantially slower-moving or stagnant fluid was seen outside the cone of filter immediately downstream of the base. Again, these differences are simply caused by the filter "legs" intersecting the measurement plane at different positions. A substantial reduction in velocity was caused by the tip of the VenaTech filter.

For each filter, the flow upstream was examined and observed to be fully developed; ie, the velocity profile was parabolic. Downstream of the filter, the flow began to return to a parabolic velocity distribution.

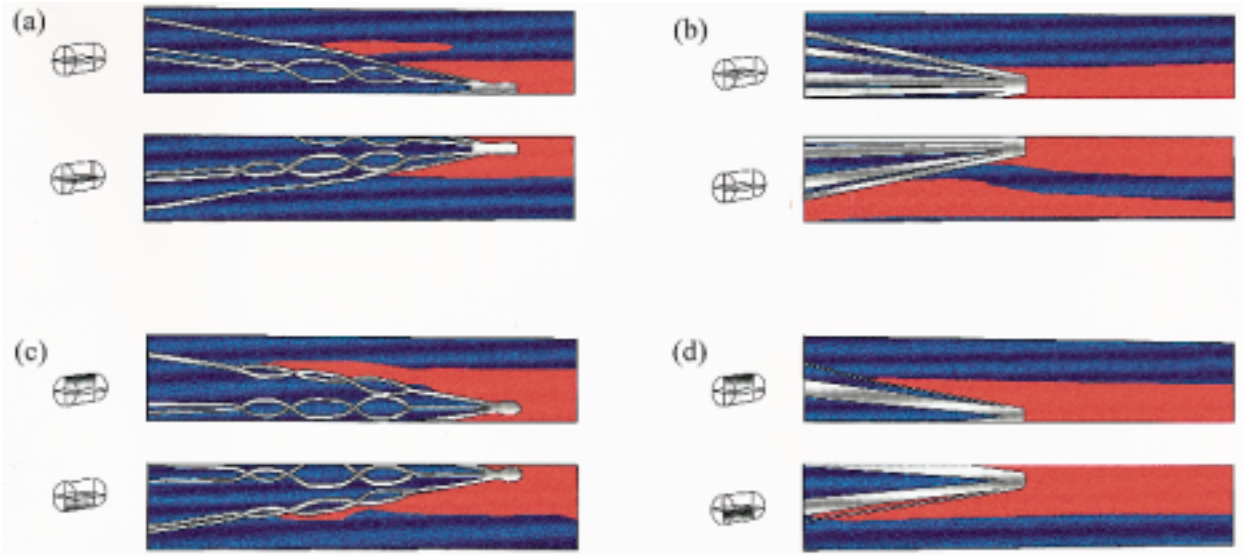

Fig 7. Regions of fluid with velocity less than the theoretically predicted value in the absence of a filter are shown in *red* for the A, horizontal and C, vertical cross-sectional planes of the 12F Titanium Greenfield filter, and the B, horizontal and D, vertical cross-sectional planes of the VenaTech LGM filter.

Wall shear stress distributions. In Fig 6, the wall shear stress distributions for the Greenfield and the VenaTech filters are shown. Wall shear stresses were calculated from the velocity profiles by fitting a cubic polynomial to several points nearest the wall or surface and computing the velocity gradient at the wall.[15-18] At each position of measurement, the magnitude of the wall shear stress was plotted in a perpendicular direction to the boundary. A positive shear stress was plotted outward from the vessel, whereas a negative value was directed inward. However, for both filters, all shear stress values measured along the vessel wall were positive, and no regions of separation or reversed flow were observed. For purposes of comparison, the theoretical wall shear stress for flow in the absence of the filter is also shown. This value is given by:

$$\tau_{ws} = \frac{32\mu Q}{\pi D^3}$$

in which Q is the flow rate, D is the diameter of the vessel, and μ is the dynamic viscosity. It is representative of the flow upstream of the filter and is based on the solution to the Navier Stokes equation for steady flow in a straight tube (ie, Poiseuille flow).

However, because of the difference in the viscosities of the test fluid and blood, the in vitro and in vivo wall shear stresses are related by:

$$\left(\frac{\tau_{ws}}{\rho\mu 2}\right)_{\text{in vivo}} = \left(\frac{\tau_{ws}}{\rho\mu^2}\right)_{\text{in vitro}}$$

Thus, the predicted in vivo wall shear stress (in vivo values are shown in brackets in Fig 6) was obtained from the values measured in vitro by multiplying by a factor of 5.

The effect of the Greenfield filter on the wall shear stress distribution along the wall was evident in all four scans shown in Fig 6, *A* and *B*, in which the experimentally measured distributions are shown in red and the upstream shear stress value is shown in black. At the base of the filter, where the "legs" have not yet influenced the flow field, the wall shear stress along the vessel wall is approximately equal to the nominal upstream value of 0.3 dyn/cm^2 or, when scaled to in vivo values, 1.5 dyn/cm^2. Downstream, the disturbance of the filter increased the wall shear stress slightly, because the flow was channeled to the region outside the cone of the filter. Continuing downstream, past the tip of the filter where the flow begins to redevelop, the wall shear stress returned to its original value. This general trend was observed in both the horizontal and vertical planes.

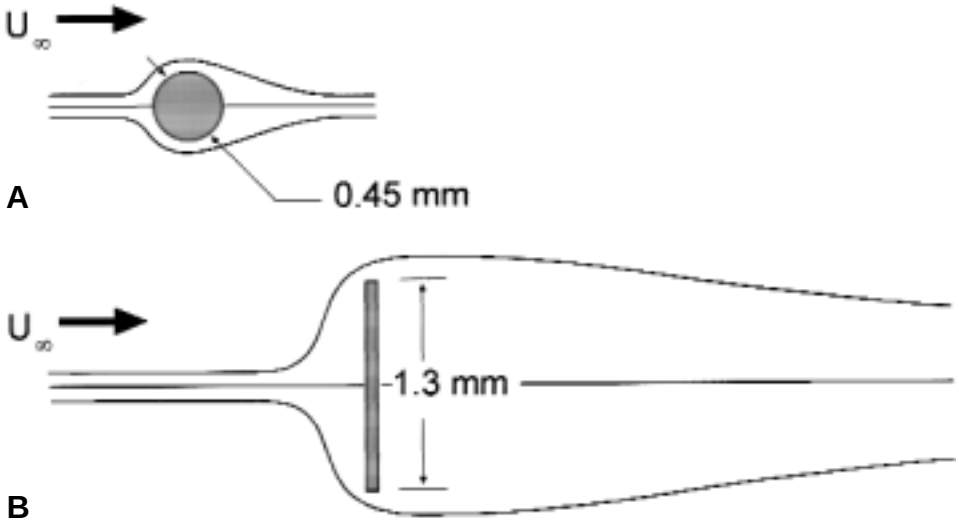

Fig 8. Sketch of streamlines showing the relative effects of flow past **A**, a round filter "leg" and **B**, a flat filter "leg."

In contrast, the wall shear distributions measured for the VenaTech filter were not nearly as symmetric as the distributions of the Greenfield filter. In the horizontal plane where the "legs" intersected the measurement plane (Fig 6, *C*), there was a considerable reduction in wall shear stress near the base of the filter. This effect is particularly noticeable in scan 3, in which the reduced levels of shear stress continue for several tube diameters downstream of the filter tip. In this case, a "leg" of the filter laid in the plane of measurement, and the fluid lying directly downstream of the leg was nearly stagnant. In the vertical plane (Fig 6, *D)*, the wall shear stress remained almost unchanged. Because the legs of the VenaTech did not intersect this particular plane of measurement, there was almost no effect on the shear stress distribution along the wall.

DISCUSSION

The observations in this study may explain the differences in rates of thrombosis and recurrent pulmonary embolism observed between the VenaTech and Greenfield filters. In a study in dogs, Qian et al[11] reported trapping rates of 76% and 43% for the VenaTech and Greenfield filters, respectively. Ricco et al found a recurrent pulmonary embolism rate of 2% and an IVC occlusion rate of 7% in a clinical trial for the VenaTech LGM filter,[20] whereas Greenfield et al found a recurrent pulmonary embolism rate of 3% with the 12F Titanium Greenfield filter.[8] A previous version of the Greenfield filter has a reported recurrent pulmonary embolism rate of 5% and an IVC occlusion rate of 3% to 5%.[2,3,6,7,21,22] Further, Mohan et al found no statistically significant difference between the 12F Titanium Greenfield and the VenaTech LGM filters' pulmonary embolism rates of 3.6% and 2% and IVC occlusion rates of 3.6% and 4%, respectively.[3] In Fig 7, the relative extents of the flow disturbances caused by the two different filters are shown. The areas in red indicate regions in which the fluid velocity was reduced below the corresponding value in the absence of the filter. In scan 1 (Fig 7, *A*), the flow disturbance caused by the intersection of a single leg of the Greenfield filter with the measurement plane is clearly seen. The disturbance dissipates within approximately 1 tube diameter or 20 mm. A similar interaction with the VenaTech filter is seen in scan 3 (Fig 7, *B*). However, the extent of the disturbed region is much greater than with the Greenfield filter. The disturbance extends downstream for approximately four tube diameters (80 mm).

Overall, the VenaTech filter has a more pronounced effect on the surrounding flow field than the Greenfield filter. Almost all the effects are caused by the respective differences in the size and shape of the supporting "legs" of the VenaTech, in comparison with the Greenfield filter. The flat "legs" used in the VenaTech filter present their largest dimension (1.3 mm) to the oncoming flow, which is nearly three times the diameter (0.45 mm) of the round "legs" of the Greenfield filter. In addition, the abrupt or sharp edges of the flat VenaTech filter "legs" result in a greater distortion of the flow field than the more streamlined Greenfield "legs."

To illustrate the different effects of these "leg" shapes on the flow field, we shall define a local Reynolds number as:

$$Re_{loc} = \frac{U_\infty d}{v}$$

in which U_∞ is the velocity of the approaching fluid, d is the effective diameter of the filter leg, and v is the kinematic viscosity. This follows the approach taken for flow past a cylinder.[19] If we consider the cross section of the round leg of the Greenfield filter placed in a uniform flow field (Fig 8*A*), as the Reynolds number is increased, the overall disturbance caused by the round leg becomes more severe, because larger vortices are generated in the wake of the "leg." However, the larger dimension of the flat VenaTech "leg" results in a larger Re_{loc} for the same upstream velocity U_∞, and with the abrupt edge of the flat VenaTech "leg," would trigger the development of vortices at a lower bulk Reynolds number, in comparison with the smaller, round "leg" of the Greenfield filter. These factors combine to cause a greater initial disturbance of the flow field and require a longer distance for its effects to dissipate and for the flow to redevelop. Although a larger frontal profile area may increase the clot-trapping efficiency of a filter, in the case of the VenaTech filter, the reduced near-wall velocities and wall-shear stresses may increase the potential for thrombogenesis and, thus, IVC occlusion. Thus, the flat shape of the VenaTech filter leg is responsible for the main differences observed in the flow fields of these two filters.

In vivo, stagnant flows produced in the shadow of the filter leg could potentially increase the chance for thrombogenesis. With the VenaTech filter, this could be enhanced by the relatively large contact area between the long supports or "feet" and the vessel wall that lies in the shadow of the filter legs. Both thrombogenesis and hyperplasia can be triggered at the vena cava wall as foreign body responses.

These differences in design suggest that although the larger cross-sectional area presented by the VenaTech filter could result in improved entrapment of smaller-sized emboli, it would come at the expense of a greater potential for thrombogenesis and IVC occlusion caused by reduced flow through a larger volume in the shadow of its legs. Thus, the Greenfield filter would be expected to have a lower incidence of IVC occlusion because of thrombosis and, thus, a higher patency rate.

The effect of the flow disturbances produced by the filter tip on filter performance is unclear. These disturbances are confined to the center of the vessel lumen. However, contrary to previous studies,[11-14] our results show no evidence of turbulence either within the filter cones or downstream of the filter tips. Even with a partially occluded Greenfield field filter, we did not observe transition to turbulence.[15] It seems that the reported turbulence was due to one of several causes. Fluid entering from the renal veins, a feature not modeled in our study, could lead to some mixing of fluid typical of turbulent flows. Also, with dye injection, secondary flows within and downstream of the filter can lead to dye streaks that can be misinterpreted.

It appears that the most likely cause of turbulence is the incorrect simulation of the in vivo flow parameters. In those in vitro studies,[11-14] the flow rate of blood in the vena cava was matched by using water at 2 L / min. Fluid dynamic similarity was not achieved, because the lower viscosity of water resulted in a mean Reynolds number of 2100, a level at which turbulence can be triggered even in a straight pipe.[19] The typical mean Reynolds number in the vena cava is 600. Qian et al used a water / glycerin mixture with a ratio of 7:1[11]; however, they did not report the viscosity or the corresponding Reynolds number.

There were some limitations associated with our simulation. First, a rigid flow model or phantom was used, in contrast to the compliant IVC. Second, a Newtonian test fluid was used. Blood is known to behave in a non-Newtonian fashion, particularly at low flow rates. However, in a vessel of this diameter, these effects will not be significant. Third, although the flow conditions in the vena cava are pulsatile, steady flow was used for these experiments to provide a basis of comparison with other studies.[11-14] Steady flow was used in these previous experiments because of the limitations of the flow visualization technique used, dye injection. Finally, the effect of inflow from iliac or renal veins was also neglected.

REFERENCES

1. Greenfield LJ, McCurdy JR, Brown PP, Elkins RC. A new intracaval filter permitting continued flow and resolution of emboli. Surgery 1973;73:599-606.
2. Greenfield LJ, Zocco J, Wilk J, Schroeder TM, Elkins RC. Clinical experience with the Kim-Ray Greenfield vena cava filter. Ann Surg 1977;185:692-8.
3. Mohan CR, Hoballah JJ, Sharp WJ, Kresowik TF, Lu CT, Corson JD. Comparative efficacy and complications of vena caval filters. J Vasc Surg 1995;21:235-46.
4. Becker DM, Philbrick JT, Selby JB. Inferior vena cava filters; Indications, safety, and effectiveness. Arch Intern Med 1992;152:1984-94.
5. Messmer JM, Greenfield LJ. Greenfield filters: Long-term radiographic follow-up study. Radiology 1985;156:613-8.

6. Pals SO, Tobin KD. Percutaneous insertion of the Greenfield filter. AJR 1989;145:827-9.
7. Greenfield LJ, Michna BA. Twelve-year clinical experience with the Greenfield vena caval filter. Surgery 1988;104:706-12.
8. Greenfield LJ, Kyung JC, Proctor M, et al. Results of a multicenter study of the modified hook-titanium Greenfield filter. J Vasc Surg 1991;14:253-7.
9. Burke PE, Michna BA, Harvey CF, Crute SL, Sobel M, Greenfield LJ. Experimental comparison of percutaneous vena caval devices: titanium Greenfield filter versus bird's nest filter. J Vasc Surg 1987;6:66-70.
10. Cimochowski GE, Evans RH, Zarins CK, Lu CT, DeMeester TR. Greenfield filter versus Mobin-Uddin umbrella. J Thorac Cardiovasc Surg 1980;79:358-65.
11. Qian Z, Yasui K, Nazarian GK, Vlodaver Z, Hunter DW, Castaneda-Zuniga WR, et al. In vitro and in vivo experimental evaluation of a new vena caval filter. J Vasc Interv Radiol 1994;5:513-8.
12. Korbin CD, Reed RA, Taylor RC, Pentecost MJ, Tietelbaum GP. Comparison of filters in an oversized vena caval phantom: Intracaval placement of a Bird's Nest Filter versus biiliac placement of Greenfield, VenaTech-LGM, and Simon Nitinol filters. J Vasc Interv Radiol 1992;3:559-64.
13. Korbin CD, Reed RA, Taylor RC, Kokoris ST, Tietelbaum GP. In vitro flow phantom analysis and clot-capturing ability of incompletely opened VenaTech-LGM vena caval filters. Cardiovasc Interv Radiol 1993;16:3-6.
14. Katsamouris AA, Waltman AC, Delichatsios MA, Athanasoulis CA. Inferior vena cava filters: in vitro comparison of clot trapping and flow dynamics. Radiology 1988;166:361-6.
15. Couch GG, Kim H, Ojha M. In vitro assessment of the hemodynamic effects of a partial occlusion in a vena cava filter. J Vasc Surg 1997;25:663-72.
16. Ojha M, Cobbold RSC, Hummel RL, Johnston KW. Pulsatile flow through constricted tubes: an experimental investigation using photochromic tracer methods J Fluid Mech 1989;203;173-97.
17. Ojha M. Spatial and temporal variations of wall shear stress within an end-to-side anastomosis model. J Biomechanics 1993;26:1377-88.
18. Ojha M. Wall shear stress temporal gradients and anastomic intimal hyperplasia. Circ Res 1994;74:1227-31.
19. Ockendon H, Ockendon JR. Viscous flow. New York: Cambridge University Press, 1995.
20. Ricco JB, Crochet D, Sebilotte P, et al. Percutaneous transvenous caval interruption with the LGM filter: early results of a multicenter trial. Ann Vasc Surg 1988;2:242-7.
21. Geisinger MA, Zelch MG, Risius B. Recurrent pulmonary embolism after Greenfield filter placement. Radiology 1987;156:383-4.
22. Wingerd M, Bernhard VM, Madisson F, Towne JB. Comparison of caval filters in the management of venous thromboembolism. Arch Surg 1978;113:1264-70.

Submitted May 19, 1999; accepted Sep 16, 1999.